PAPER

Equivalent circuit modeling of the ac response of Pd-ZrO_2 granular metal thin films using impedance spectroscopy

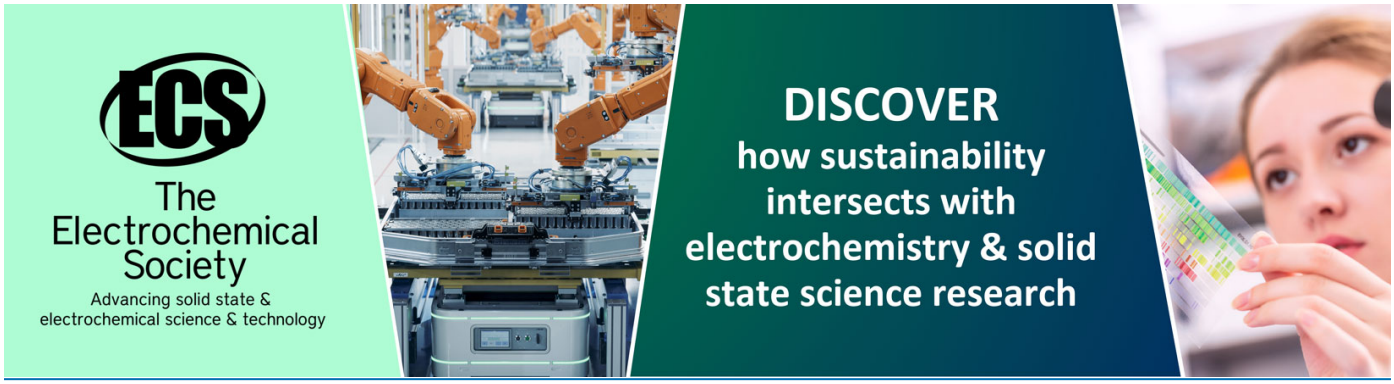

IOP Publishing Journal of Physics D: Applied Physics
J. Phys. D: Appl. Phys. **48** (2015) 335306 (7pp) doi:10.1088/0022-3727/48/33/335306

Equivalent circuit modeling of the ac response of Pd-ZrO_2 granular metal thin films using impedance spectroscopy

Hicham Bakkali[1,2], Manuel Dominguez[1], Xavier Batlle[2] and Amílcar Labarta[2]

[1] Departamento de Física de la Materia Condensada and Instituto de Microscopía Electrónica y Materiales, Universidad de Cádiz—11510 Puerto Real, Cádiz, Spain
[2] Departament de Física Fonamental and Institut de Nanociència i Nanotecnologia, Universitat de Barcelona—Avinguda Diagonal 647, 08028 Barcelona, Catalonia, Spain

E-mail: hicham.bakkali@mail.uca.es

Received 16 January 2015, revised 23 June 2015
Accepted for publication 29 June 2015
Published 22 July 2015

Abstract

The ac response in the dielectric regime of thin films consisting of Pd nanoparticles embedded in a ZrO_2 insulating matrix, fabricated by co-sputtering, was obtained from impedance spectroscopy measurements (11 Hz–2 MHz) in the temperature range 30–290 K. The response was fitted to an equivalent circuit model whose parameters were evaluated assuming that, as a consequence of the bimodal size distribution of the Pd particles, two mechanisms appear. At low frequencies, a first element similar to a parallel RC circuit dominates the response, due to two competing paths. One of them is associated with thermally-activated tunneling conductance among most of the smallest Pd particles (size ~ 2 nm), which make up the dc tunneling backbone of the sample. The other one is related to the conductance associated with the capacitive paths among larger Pd particles (size > 5 nm). At low temperature and intermediate frequencies (~1 kHz), a shortcut process between the larger particles connects regions initially isolated from the backbone at low frequencies. These regions, populated by some additional smaller particles located around two bigger particles, were isolated because the bigger particles separation is too large for the tunneling current. Once connected to the backbone, current may also flow through them by means of the so-called thermally-activated assisted tunneling resistive paths, yielding the second element of the equivalent circuit (a parallel RLC element). At high temperature, the thermal energy shifts the onset of the shortcut process high frequencies and, thus, only the first element is observed. Considering these results, controlling the particle size distribution could be helpful to tune up the frequency at which tunneling conductance dominates the ac response of these granular metals.

Keywords: granular metals, ac transport properties, impedance spectroscopy

(Some figures may appear in colour only in the online journal)

Introduction

Granular metals, containing metallic nanoparticles embedded in a dielectric amorphous matrix, are of major importance for material science because of their transport properties [1–7]. These materials exhibit promising optical applications [8, 9], associated with their large third-order non-linear susceptibility [10, 11], ultra fast response [12], several biomedical applications [13] and, when the nanoparticles are magnetic, some interesting applications as high coercive films for information storage and high permeability materials in the form of thin films [14–16] for electromagnetic shield protecting against high frequency electromagnetic radiation [17]. Particularly, Pd embedded in a zirconia insulating matrix, being an oxide

material of high chemical potential, have been reported to be very active and stable [18], as well as a good way to obtain Pd nanoparticles with a high probability of tunneling conductance through them. These composites are potentially applied as electrodes in solid oxide fuel cells (SOFC) and oxygen sensors [19].

Granular metals show quite different transport properties, depending on the volume fraction x of the metallic nanoparticles. We focus on studying the situation when x is less than the percolation threshold, that is, the material is in the dielectric regime and most of the particles are isolated [6, 7, 20]. A broad understanding of the dc transport properties of these nanomaterials has been reached concluding that their behavior is based in thermally-activated tunneling [4–7, 20–23]. However, ac electrical transport is mainly due to two distinct processes: the quantum tunneling process of electrons between nanoparticles separated not more than a few nanometers, which is temperature-dependent [20, 21], and capacity conductance between the charged surfaces of neighboring particles. So far, the study of the ac response and optical properties of granular metals has been mainly focused on systems for which the tunneling process is negligible and, as a consequence, there is still no satisfactory explanation for the ac response of these materials in the limit at which conduction by tunnel effect and by capacitance between particles are almost of the same magnitude [23]. Impedance spectroscopy has been reported to be of great interest to study the electrical properties derived from grain boundaries in these nanomaterials [24–26]. This technique may reveal the relative variation of electrical conduction paths, and can efficiently clarify the inter-granular electrical barrier and the origin of resistance or capacitance in homogeneous composite films [27].

In this paper, we report on temperature dependence of the impedance and phase angle of the ac properties up to high frequency of Pd-ZrO_2 granular thin films with competing tunneling and capacitive channels throughout the system. The electrical response of the films is modeled by a one-dimensional (1D) geometrical structure, being the sample thickness comparable to the Pd nanoparticles size. The grain boundary regions are assumed to be connected in series by a parallel combination of tunneling effective resistance $R_{t/\mathrm{eff}} = \sum_i R_{t_i}$ and effective capacitance $1/C_{s/\mathrm{eff}} = \sum_i 1/C_{s_i}$ through the set of the smaller particles, and by an effective capacitance given by $1/C_{b/\mathrm{eff}} = \sum_i 1/C_{b_i}$ through the set of the larger particles not electrically connected by tunneling, being R_{t_i},C_{s_i} and C_{b_i}, the tunneling resistance between two small particles, capacitance between two small particles and the capacitance between two larger particles, respectively.

Experimental

Pd-ZrO_2 samples were evaporated on SiO_2 substrates by co-sputtering of Pd and ZrO_2 stabilized with 7% volume yttrium oxide (Y_2O_3) targets, using magnetron sputtering (MS). The distance between the target and sample was fixed at 10.7 cm, Ar pressure was 2.3×10^{-2} mbar, sample exposure time was 30 s, film thickness was 10 nm and the deposition power was 30 watt for Pd and 255 watts for ZrO_2. After deposition of the Pd-ZrO_2 layer, four parallel Au strips were thermally evaporated on the sample surface to provide the metallic contacts for four-point electrical measurements. These strips were approximately 5 mm long, 1 mm wide, and were separated by a distance of 0.7 mm. The films were initially characterized with a JEOL 2010 high resolution transmission electron microscopy (HRTEM) for structural analysis, where the images were digitally treated with Digital Micrograph software [28]. The elemental analysis was performed by energy dispersive x-ray microanalysis (EDX), leading to $x = 0.28$. The modulus of complex impedance ($|Z(\omega)|$) and the phase angle were measured in the frequency range of 11 Hz to 2 MHz in the temperature range of 30–290 K, using a precision LCR Meter (QuadTech 7600 Plus), a KEITHLEY 6221 ac current source and, KEITHLEY 2182A Nano-Voltmeter in a continuous-flow He cryostat. The computer analysis method used to fit the Impedance Spectroscopy data to their equivalent circuits model was a complex nonlinear least squares fitting (CNLS package), in which all parameters of the fitting model are adjusted simultaneously to produce an optimal fit to the data [29].

Results and discussion

Figure 1(a) shows HRTEM images of Pd-ZrO_2 thin films. Dark regions correspond to Pd nanoparticles and light regions to the amorphous ZrO_2 matrix. The particles are spherical in shape. In the histogram in figure 1(c) a bimodal size distribution of Pd particles is observed, with one peak centered at smaller sizes (~2 nm) and the other (less clear) at larger sizes (>5 nm). Figure 1(b) shows magnification of a set of particles. The particles are crystalline since they exhibit lattice contrast corresponding to the atomic planes and diffraction pattern was indexed to the expected fcc Pd structure. Lattice contrast is not present in the ZrO_2 matrix suggesting that it is amorphous. The average distance among the smaller particles is of about one nanometer, which is excellent for tunneling conductance [30], because of their corresponding low tunnel barrier. In contrast, larger particles are farther apart (> 3 nm), producing high tunnel barriers and, therefore, they do not contribute to the tunneling channels. These observations are in good agreement with the assumption proposed by Abeles and co-workers [20, 21, 30] concerning the uniformity of the metallic phase in granular films, such that the relationship between the diameter particles d and the interparticle distance D is constant for similarly-sized particles. Moreover, as the capacitance between two identical particles is proportional to d^2/D, it is also proportional to d, as d/D is constant. As a consequence, the contribution to the capacitive conductance is considered to be dominated by the larger particles, which have a much smaller impedance than that of the smaller particles. Here, it is worth noting that $\sum_i 1/C_{s_i} \gg \sum_i 1/C_{b_i}$, being C_{s_i} and C_{b_i} the average capacitance between small and large particles, respectively.

Figure 2 shows that, at low frequencies near 10 Hz, Z increases as the temperature decreases, suggesting the presence of thermally activated tunneling due to the dc conductance

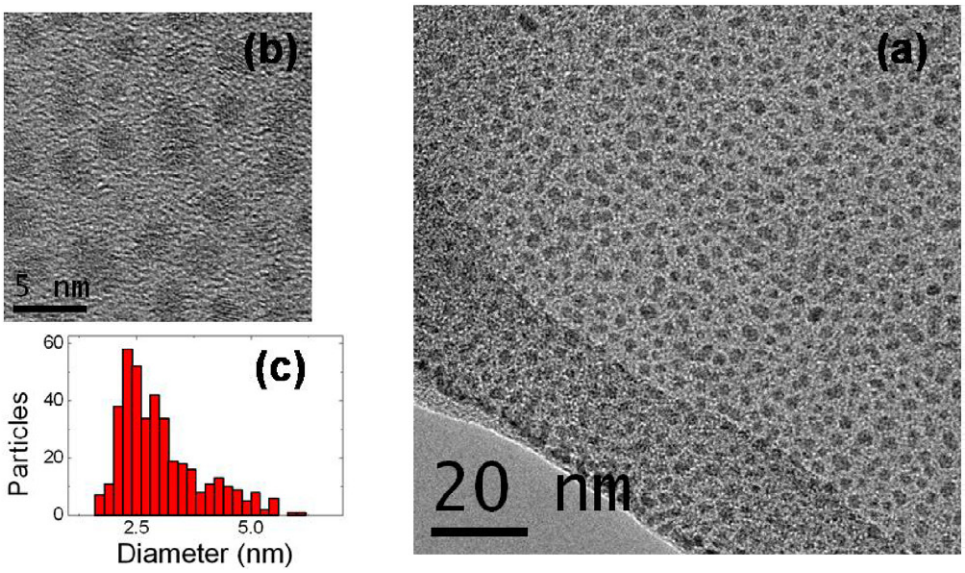

Figure 1. (a) HRTEM micrograph of granular Pd-ZrO_2 with metallic volume fraction $x = 0.28$; (b) HRTEM showing the crystalline nature of the Pd nanoparticles; (c) distribution of particle sizes obtained by analyzing a set of HRTEM micrographs.

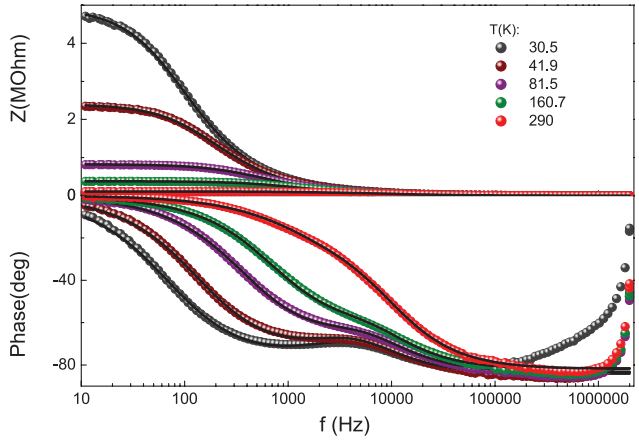

Figure 2. Impedance modulus and phase angle of Pd-ZrO_2 granular thin film as a function of frequency in the temperature range 30–290 K. Solid lines show the fitting of experimental data to equation (1).

of the sample [22]. At low frequency, the phase angle is negligible because the electrons flow almost exclusively by tunneling through resistive paths among the smaller particles. As frequency increases, the capacitive effect becomes more noticeable and, thus, Z decreases and the phase angle becomes negative and approaches −90° for the whole temperature range. This dependence can be explained in terms of a competition between parallel tunneling (resistive) and capacitive paths in the metallic particles.

At frequencies of the order and higher than 1 kHz, a constant phase angle regime (CPAR) [23, 31] is observed, which is more pronounced at low temperature. The onset of the CPAR is related to the frequency at which the conductance of direct tunneling paths and that of the parallel capacitance paths becomes comparable. As frequency increases, current starts to flow only through the capacitive channels among the larger particles, leading to the appearance of a random shortcut capacitor network throughout the sample. This effect improves the electrical conductance by giving way to new paths mediated by assisted tunneling conduction among particles initially isolated at low frequencies, which compensates for the phase reduction and, consequently, the phase angle remains constant.

CPAR extends for a certain range of frequencies until it is abandoned by further increasing frequency, since the capacitance between larger particles becomes comparable to the total tunnel-assisted resistance, thus increasing the capacitive nature of the whole sample. CPAR shifts to higher frequency with increasing temperature until it disappears at room temperature (T = 290 K), due to the smaller relative contribution of the capacitive shortcut with respect to the contribution of thermally-activated, direct-tunneling resistance [31]. At frequencies greater than about 100 kHz, the phase angle begins to deviate from the predicted flattening towards −90° and increases quickly backwards to zero. This anomalous behavior is not caused by any intrinsic phenomena in the granular system but it arises from the significant contribution at such high frequencies of the measuring leads and electrodes and the high electrical losses associated with them [32, 33].

The impedance spectra of Pd-ZrO_2 at different temperatures are shown in figure 3 in the form of a Cole–Cole plot. At the temperature range of 30–160 K, the spectra show two partially overlapping semicircles with different orders of magnitude in their relaxation times and, thus, the small high-frequency arc is obscured by the larger low-frequency arc. The electrical response due to the electrodes is negligible in most of the frequency range in figure 3, since its corresponding arc is not observed in any of the spectra, indicating the electronic conductive nature of Pd-ZrO_2 films [24]. The response at low frequencies completely dominates these plots, making it difficult to resolve the high frequency response, even when the high frequency end is expanded, as in the inset to figure 3.

In these cases, it is helpful to use the complex electric modulus ($|M(\omega)|$) to resolve the different relaxation processes, in which the semicircles can be scaled inversely to

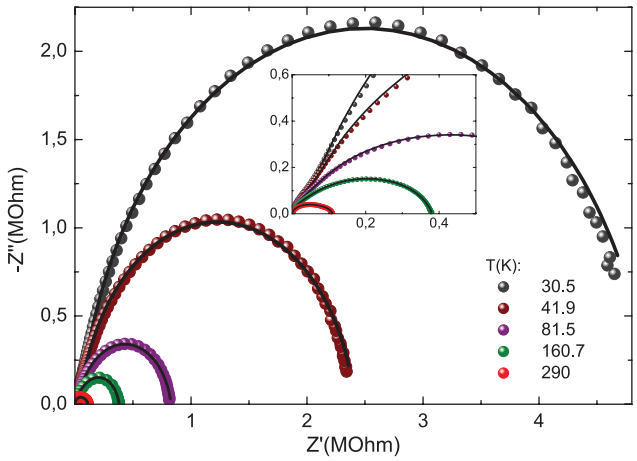

Figure 3. Impedance spectra of Pd-ZrO_2 thin film (Cole–Cole plot) $-Z''$ versus Z', measured at different temperatures, in the frequency range of 11 Hz to 100 kHz. Solid lines show the fitting of experimental data to equation (1). The inset shows the high frequency end of these plots.

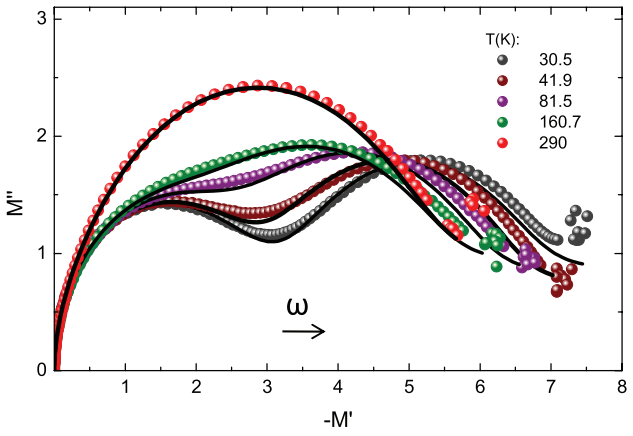

Figure 4. Complex modulus plots of Pd-ZrO_2 thin films, M'' versus $-M'$, measured at different temperatures, in the frequency range of 11 Hz to 100 kHz. Solid lines show the fitting of experimental data to equation (1). Two semicircles are clearly shown while, at room temperature, only one semicircle is observed.

the capacitance [34]. The real and imaginary parts values of $M(\omega)$ are, respectively, calculated using $M'(\omega) = \omega C_0 Z''$, and $M''(\omega) = \omega C_0 Z'$, and they are plotted in a Cole–Cole plot as shown in figure 4, where C_0 is the geometrical capacitance, $C_0 = \varepsilon_0 A/d$, $\varepsilon_0 = 8.854 \times 10^{-12}\,\mathrm{Fm}^{-1}$ is the vacuum permittivity, $A = 50 \times 10^{-12}\,\mathrm{m}^2$ is the electrode area, and $d = 7 \times 10^{-4}\,\mathrm{m}$ is the electrode separation. In the low temperature range of 30–160 K, two arcs are clearly observed in figure 4, indicating two different relaxation processes, while at room temperature, only one relaxation process is observed throughout the whole frequency range. These observations are in accordance with those hardly observed previously in the complex impedance spectra of figure 3, especially at the high frequency end. Those two semicircles exhibit Debye-like peaks with characteristic frequency maxima $f_{1\,\max}$ and $f_{2\,\max}$, corresponding to the low frequency and high frequency semicircles, respectively, thus suggesting the occurrence of two different absorption processes [35] related to two different relaxation times $\tau_1 = 1/f_{1\,\max}$ and $\tau_2 = 1/f_{2\,\max}$, respectively. In figure 5, a plot of $\tau(T)$ versus $T^{-1/2}$ shows that the characteristic relaxation time is well described by the typical model of granular films following thermal activation $\tau(T) \propto \exp\left(2\sqrt{W/K_B T}\right)$ [21]. The activation energy W is directly related to the Coulomb charging energy of the particles E_c, $W = E_C d\chi$, d being the interparticle distance associated with the smaller particles and χ the tunneling barrier energy in units of wave vector. The characteristic $T^{-1/2}$ dependence is a distinct signature of grain size uniformity ($d/D \sim$ constant) [36]. We obtain an experimental value of ~ 12 meV and ~ 0.8 meV for W_1 and W_2, respectively.

The low frequency response is due to the competition of direct tunneling among the smaller particles and capacitive paths among the larger particles. At small frequencies, $f \to 0$ Hz the current flows exclusively by direct tunneling channels being $R_{\mathrm{td/eff}}$ the direct tunneling resistance. In this case, the measured resistance is the same as in dc (direct current) measurements previously reported [22]. For comparison,

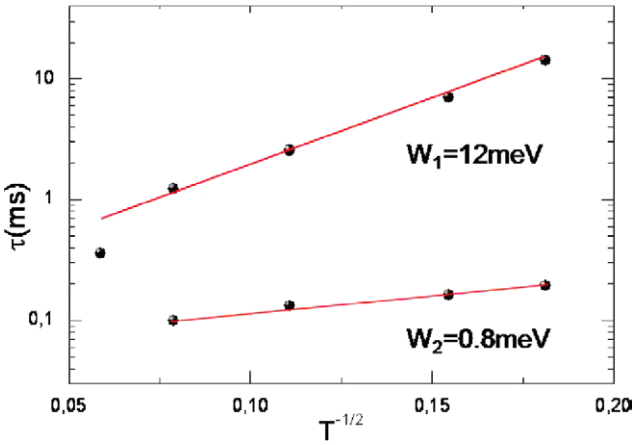

Figure 5. Temperature dependence of the relaxation times τ_1 and τ_2, obtained from fitting experimental data in figure 4 to equation (1). The solid lines stand for linear fit of data. W_1 and W_2 are the corresponding thermal activation energies.

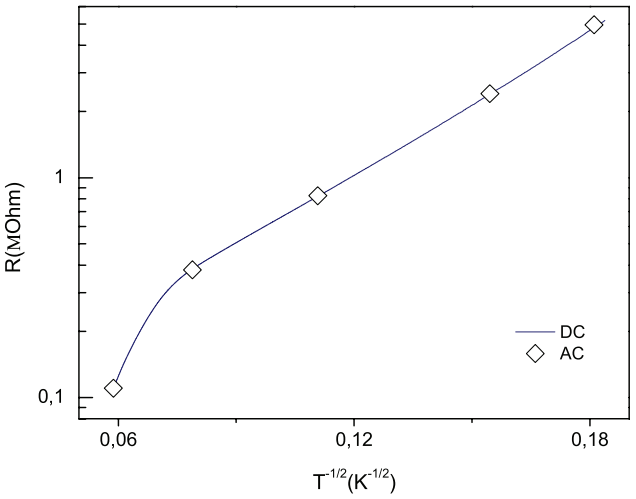

Figure 6. dc resistance of the sample and low frequency impedance plotted versus $T^{-1/2}$.

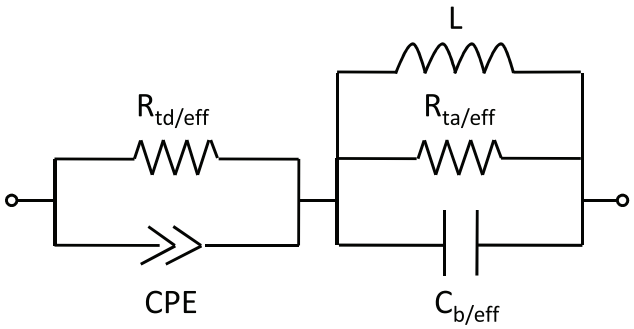

Figure 7. Electrical equivalent circuit model of Pd-ZrO_2 granular thin films with a bimodal distribution of particle sizes.

figure 6 shows dc resistance and low frequency impedance as a function of temperature. As frequency increases, the current begins to flow in parallel through an effective capacitance among large particles, $C_{b/\mathrm{eff}}$, until the conductance of both tunneling and capacitive channels becomes comparable, $R_{\mathrm{td}/e\mathrm{ff}}^{-1} \approx \omega_{1\,\max} C_{b/\mathrm{eff}}$ (upper part of the first semicircle). When the frequency further increases, the admittance, resulting from the capacitor element $C_{b/\mathrm{eff}}$ also increases, until shortcuts between bigger particles are randomly inserted into the sample. These short-circuited big particles can be considered as nano-electrodes connecting regions with small particles previously isolated from the dc tunneling backbone of the sample. This shortcut leads to assisted tunneling processes among small particles, being $R_{\mathrm{ta/eff}}$ the effective tunneling resistance of the initially isolated smaller particles, and results in the onset of the second semicircle. This process is called 'assisted tunneling' because it requires the previous shortcut of bigger particles to appear, although it is the same physical process shown by the smaller particles in the tunneling backbone. Actually, the second semicircle observed at high frequency only represents an additional response of the sample. In the same way as before, when the frequency continues increasing, the current flows back again in parallel through $R_{\mathrm{ta/eff}}$ and $C_{b/\mathrm{eff}}$ until the conductance of both tunneling and capacitive channels becomes comparable $R_{\mathrm{ta/eff}}^{-1} \approx \omega_{2\,\max} C_{b/\mathrm{eff}}$ (upper side of the second semicircle). This second competition of tunneling-assisted and capacitive paths is observed since the effective resistance of the set of the smaller particles involved in the tunneling-assisted process is much smaller than of that involved in the direct tunneling process $R_{\mathrm{ta/eff}} \langle\langle R_{\mathrm{td/eff}}$. As the frequency further increases, the capacitor admittance corresponding to $C_{b/\mathrm{eff}}$ continues to increase and the current flows only through the capacitive channels among the larger particles, therefore, the capacitive natures of the total current increases and the phase angle becomes more negative. Consequently, the maximum of the low frequency semicircle corresponds to the $R_{\mathrm{td/eff}} C_{b/\mathrm{eff}}$ response while the high frequency semicircle corresponds to the $R_{\mathrm{ta/eff}} C_{b/\mathrm{eff}}$ one.

Impedance spectroscopy results are thus well modeled by an equivalent circuit containing two elements in series as sketched in figure 7. The first part of the circuit comprises a resistor $R_{\mathrm{td/eff}}$, in parallel with a constant phase element (CPE) associated with the bigger particles capacitance, whose impedance is given by $Z(CPE) = 1/Q(j\omega)^{\phi}$ [37], where Q and ϕ are fitting parameters, and ω is the angular frequency. CPE is used to enhance the process of fitting the impedance data since, for materials with distributed properties, the impedance of the equivalent circuit cannot be approximated only by a finite number of ordinary sets of constant elements [37]. Thus, CPE is an equivalent circuit component that models the behavior of an imperfect capacitor or inductor, which produces an impedance having a constant phase angle in the complex plane. The exponent ϕ determines this angle which is $\frac{\pi}{2} \cdot \phi$ with ϕ ranging from −1 to +1. From our fitting parameters, ϕ is near +1, concluding that this CPE is modeling here an imperfect capacitor. Moreover, the second part of the equivalent circuit comprises three parallel elements ($R_{\mathrm{ta/eff}} L C_{b/\mathrm{eff}}$). Therefore, the complex impedance of the equivalent circuit can be written as:

$$Z(\omega) = \frac{R_{\mathrm{td/eff}}}{1 + R_{\mathrm{td/eff}} Q(j\omega)^{\phi}} + \frac{R_{\mathrm{ta/eff}}[1 - j(\omega C_{b/\mathrm{eff}} - 1/\omega L) R_{\mathrm{ta/eff}}]}{1 + (\omega C_{b/\mathrm{eff}} - 1/\omega L)^2 R_2^2}. \quad (1)$$

Experimental impedance in figure 2, and corresponding impedance spectra in figures 3 and 4, are fitted to equation (1) and the fitted parameters are given in table 1. The following approximations have been assumed. At low frequency, $f \to 0$ Hz, it can be noted that in the first term of equation (1), the impedance of the CPE term is far greater than that of $R_{\mathrm{td/eff}}$, while the second term of equation (1) is negligible. We can therefore assume that the effective impedance of the circuit can be expressed as $Z(\omega \to 0) \approx R_{\mathrm{td/eff}}$ leading to the low frequency conductance (dc conduction) and mainly reveals the smaller particles contribution. The plots of $R_{\mathrm{td/eff}}(T)$ and $R_{\mathrm{ta/eff}}(T)$ versus $T^{-1/2}$ extracted from fitting data in table 1 (see figure 8), are well described by the expected model of granular thin films following thermal activation tunneling, where the temperature dependence of the dc resistance reads $R(T) \propto \exp\left(2\sqrt{B/K_{\mathrm{B}}T}\right)$ [21]. We obtained experimental values $B_1 \sim 13$ meV and $B_2 \sim 0.7$ meV associated with $R_{\mathrm{td/eff}}(T)$ and $R_{\mathrm{ta/eff}}(T)$, respectively. These values are in relatively good agreement with those obtained from τ_1 and τ_2. It is reasonable to expect that B and W values are comparable confirming that R and τ have the same temperature dependence on $T^{-1/2}$, since $\omega_{\max} \approx \left(1/R_{t/\mathrm{eff}} C_{b/\mathrm{eff}}\right) \propto 1/R_{t/\mathrm{eff}}$, $C_{b/\mathrm{eff}}$ being almost constant.

Furthermore, at room temperature, experimental data in figures 2–4 are fitted only with the first part of the equivalent circuit shown in figure 7 throughout the whole frequency range ($f = 11$ Hz–2 MHz). This could be explained by the absence of the contribution of the assisted tunneling resistance, since at high temperatures the value of the effective direct tunneling resistance decreases thus favoring the current flow through the resistive backbone. This effect shifts the shortcut processes through bigger particles towards higher frequencies, beyond our frequency range of measurement. Therefore, only the first part of the circuit is considered at room temperature, as the second part of the equation can be neglected. Then, equation (1) is simply reduced to equation (2):

Table 1. Fitting parameters of the equivalent circuit model in equation (1) for the experimental impedance values shown in figure 2, in the temperature range 30–290 K.

$T(K)$	$R_{td/eff}(\Omega)$	$Q(s^{\phi}/\Omega)$	ϕ(rad)	$C_{b/eff}(F)$from$Q$	$f_{1\,max}$(Hz)	$R_{ta/eff}(\Omega)$	$C_{b/eff}(F)$	$f_{2\,max}(Hz)$	$L(H)$
30.5	4.9×10^{6}	7.8×10^{-10}	0.914	4.6×10^{-10}	70	5.92×10^{4}	5.2×10^{-10}	5200	867
41.9	2.4×10^{6}	8.4×10^{-10}	0.914	4.7×10^{-10}	142	5.20×10^{4}	5×10^{-10}	6100	492
81.5	8.2×10^{5}	1.03×10^{-9}	0.906	4.0×10^{-10}	391	4.17×10^{4}	5×10^{-10}	7600	92
160.7	3.8×10^{5}	1.10×10^{-9}	0.912	5.2×10^{-10}	807	3.18×10^{4}	5×10^{-10}	10000	11
290	1.1×10^{5}	1.80×10^{-9}	0.873	5.2×10^{-10}	2762	...	...	...	...

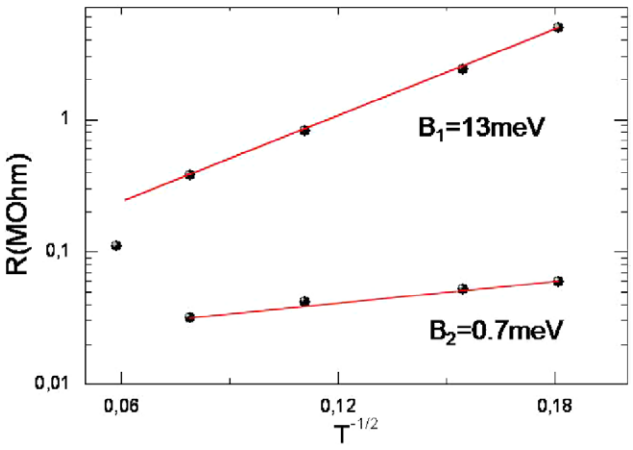

Figure 8. Temperature dependence of the real part of impedance $R_{td/eff}(0, T)$ at low frequencies, $f \to 0$ Hz, obtained from fitting experimental data in figure 4 to equation (1). The solid lines stand for a linear fit of $R_{td/eff}(0, T)$ to the thermally-activated tunneling conductance of the Abeles model. B_1 and B_2 are the corresponding thermal activation energies.

$$Z(\omega) = \frac{R_{td/eff}}{1 + R_{td/eff}Q(j\omega)^{\phi}}. \quad (2)$$

The values of each equivalent circuit component ($R_{td/eff}, R_{ta/eff}, CPE, C_{b/eff}, L$) are shown in table 1. The values obtained are in good agreement with the previously discussed in the ac response of the sample. Considering that the grain boundary regions are assumed to be connected in series in our model, the effective capacitance associated with the *CPE* can be expressed as $C_{b/eff} = Q^{1/\phi}R_{td/eff}{}^{(1-\phi)/\phi}$ when $\phi\langle 1$ [38]. The capacitance values extracted from Q in the previous equation for the first semicircle are comparable to those directly obtained from the second semicircle, as shown in table 1. This confirms our previous hypothesis concerning the capacitive conduction process, which is expected to be dominated by the larger particles. The presence of a small inductive contribution in the equivalent circuit may reveal the helical path of charge carriers percolating between the larger particles, as has been suggested for similar granular systems [39]. Here, it is worth noting that the inductance L does not contribute to the relaxation time dispersion.

Conclusions

The impedance spectra of granular thin films of Pd-ZrO_2 in the dielectric regime have been studied. The ac electrical response has been well modeled by an equivalent circuit which involves two distributed elements, arising from the contribution of small (~2 nm) and large (> 5 nm) Pd particles. Two absorption phenomena are found, which are related to competing, thermally-activated tunneling and capacitive paths. The low frequency absorption is associated with the competition between direct tunneling channels through the smaller particles and capacitive paths through the larger particles; the high frequency absorption is associated with the additional contribution of tunneling-assisted conductance through regions of the sample, initially disconnected from the electrical backbone at lower frequencies, by means of the capacitive shortcuts among the larger particles. At room temperature, the second dispersive region is not observed since, as temperature increases, the value of direct tunneling resistance decreases and it shifts the first absorption processes towards frequencies above our experimental range. Taking into account that in previous experimental and theoretical works the electrical behavior of granular films was modeled by a resistor-capacitor random network [23, 31, 40], in this study we have proposed the use of the complex nonlinear least square fitting method to obtain a simple equivalent circuit model for the overall system, throughout the whole temperature range. All the foregoing may be observed because of the bimodal size distribution of Pd particles, which suggests that the latter fully determines the ac electrical response of granular metals in the dielectric regime.

Acknowledgments

This work was supported by the Spanish MICINN (H.Bakkali Ph.D. Grant No. BES-2008–010141 and research project MAT2012-33037), European FEDER funds (Una manera de hacer Europa) and the Catalan DURSI (2009SGR876, 2014SGR220). Dr M Kovylina (UB) is acknowledged for sample preparation.

References

[1] Ohnuma S, Fujimori H, Mitani S and Masumoto T 1996 *J. Appl. Phys.* **79** 5130
[2] Yu M, Liu Y, Moser A, Weller D and Sellmeyer D J 1999 *Appl. Phys. Lett.* **75** 3992
[3] Watanabe W, Masumoto T, Ping D H and Hono K 2000 *Appl. Phys. Lett.* **76** 3971
[4] Batlle X and Labarta A 2002 *J. Phys. D: Appl. Phys.* **35** R15
[5] Hattink B J, García del Muro M, Konstantinović Z, Batlle X, Labarta A and Varela M 2006 *Phys. Rev.* B **73** 045418

[6] Konstantinović Z, García del Muro M, Varela M, Batlle X and Labarta A 2006 *Nanotechnology* **17** 4106
[7] Konstantinović Z, García del Muro M, Kovylina M, Batlle X and Labarta A 2009 *Phys. Rev.* B **79** 094201
[8] Hamanaka Y, Fukuta K, Nakamura A, Liz-Marzán L M and Mulvaney P 2004 *Appl. Phys. Lett.* **84** 4938
[9] Maaza M, Nemraoui O, Sella C, Beye A C and Baruch-Barak B 2005 *Opt. Commun.* **254** 188
[10] Cummings K D, Garland J C and Tanner D B 1984 *Phys. Rev.* B **30** 4170
[11] Sharma A K, Muth J F, Kvit A, Narayan J and Kolbas R M 2000 *Mat. Res. Soc. Symp.* **617** J2.7.1
[12] Polman A, Snoeks E, van den Hoven G N, Brongersma M L, Serna R, Shin J H, Kiki P and Radius E 1995 *Nucl. Instrum. Methods* B **106** 393
[13] Tartaj P, del Puerto Morales M, Veintemillas Verdaguer S, Gonzalez-Carreno T and Serna C J 2003 *J. Phys. D: Appl. Phys* **36** R182
[14] Stavroyiannis S, Panagiotopoulos I, Niarchos D, Christodoulides J A, Zhang Y and Hadjipanayis G C 1999 *J. Appl. Phys.* **85** 4304
[15] Yu M, Liu Y, Moser A, Weller D and Sellmyer D J 1999 *Appl. Phys. Lett.* **75** 3992
[16] Watanabe M, Masumoto T, Ping D H and Hono K 2000 *Appl. Phys. Lett.* **76** 3971
[17] Bader S D 2002 *Science* **500** 172–88
[18] Epling W and Hoflund G 1999 *J. Catal.* **182** 5
[19] Torres-Huerta A M *et al* 2007 *Solid State Ion.* **178** 1608
[20] Abeles B, Sheng P, Coutts M D and Arie Y 1975 *Adv. Phys.* **24** 407
[21] Abeles, P Sheng M D and Arie Y 1973 *Phys. Rev. Lett.* **31** 44
[22] Bakkali H and Dominguez M 2013 *Europhys. Lett.* **104** 17007
[23] Hattink B J, Labarta A, García del Muro M, Batlle X, Sánchez F and Varela M 2003 *Phys. Rev.* B **67** 033402
[24] Chiang Y M, Lavik E B and Blom D A 1997 *Nanostruct. Mater.* **9** 633
[25] Lee J, Hwang J H, Mashek J J, Mason T O, Miller A E and Siegel R W 1995 *J. Mater. Res.* **10** 2295
[26] Puin W and Heitjans P 1995 *Nanostruct. Mater.* **6** 885
[27] Macdonald J R 1987 *Impedance Spectroscopy* (New York: Wiley)
[28] Hovden R 2012 *Microsc. Today* **20** 24
[29] Macdonald J R and Garber J A 1977 *J. Electrochem. Soc.* **124** 1022
[30] Mitani S, Takahashi S, Takahashi K, Yakushiji K, Maekawa S and Fujimori H 1998 *Phys. Rev. Lett.* **81** 2799
[31] Konstantinovic Z, García del Muro M, Batlle X and Labarta A 2007 *Appl. Phys. Lett.* **91** 052108
[32] Srivastava A, Garg A and Morrison F D 2009 *J. Appl. Phys.* **105** 054103
[33] Schmidt R, Eerenstein W, Winiecki T, Morrison F D and Midgley P A 2007 *Phys. Rev.* B **75** 245111
[34] Morrison F D, Sinclair D C and West A R 2001 *J. Am. Ceram. Soc.* **84** 531
[35] Jonscher A N 1999 *J. Phys. D: Appl. Phys.* **32** R57
[36] Black C T, Murray C B, Sandstrom R L and Shouheng S 2000 *Science* **290** 1131
[37] Barsoukov E and MacDonald J R (ed) 2005 *Impedance Spectroscopy: Theory, Experimental, and Applications* (Hoboken, NJ: Wiley-Interscience)
[38] Hirschorn B *et al* 2010 *Electrochim. Acta* **55** 6218–27
[39] Koltunowicz T, Zhkovski P, Bury P, Larkin A, Fedotov A and Fedotov J 2012 *Electr. Rev.* **88** 93–5
[40] Almond D P and Vainas B 1999 *J. Phys.: Condens. Matter* **11** 9081